Triple threshold lasing from a photonic trap in a Te/Se-based optical microcavity

Krzysztof Sawicki [1], Jean-Guy Rousset [1], Rafał Rudniewski [1], Wojciech Pacuski [1], Maciej Ściesiek [1], Tomasz Kazimierczuk [1], Kamil Sobczak [2], Jolanta Borysiuk [1], Michał Nawrocki[1] & Jan Suffczyński [1]

Lasing relies on light amplification in the active medium of an optical resonator. There are three lasing regimes in the emission from a quantum well coupled to a semiconductor microcavity. Polariton lasing in the strong light–matter coupling regime arises from the stimulated scattering of exciton-polaritons. Photon lasing in the weak coupling regime relies on either of two mechanisms: the stimulated recombination of excitons, or of an electron–hole plasma. So far, only one or two out of these three regimes have been reported for a given structure, independently of the material system studied. Here, we report on all three lasing regimes and provide evidence for a three-threshold behavior in the emission from a photonic trap in a Se/Te-based planar microcavity comprising a single CdSe/(Cd,Mg)Se quantum well. Our work establishes the so far unsettled relation between lasing regimes that differ by their light-matter coupling strength and degree of electron–hole Coulomb correlation.

[1] Institute of Experimental Physics, Faculty of Physics, University of Warsaw, Pasteura St. 5, 02-093 Warsaw, Poland. [2] Biological and Chemical Research Centre, University of Warsaw, Żwirki i Wigury St. 101, 02-089 Warsaw, Poland. Deceased: Michał Nawrocki. Correspondence and requests for materials should be addressed to J.Sńs. (email: Jan.Suffczynski@fuw.edu.pl)

Carriers and photon confinement in semiconductor nano- and microstructures bring a variety of fascinating linear and non-linear phenomena, such as optical parametric oscillation[1] and polariton superfluidity[2]. Among the non-linear phenomena, lasing effects attract a considerable attention, in particular, due to their direct implications toward practical use. Depending on the strength of the light–matter coupling and the electron–hole interaction, three regimes of coherent light generation in a semiconductor microcavity can be distinguished. In the strong light–matter coupling regime, coherent light emission results from the stimulated scattering and radiative decay of mixed photon–exciton states called exciton-polaritons[3–5]. In the weak coupling regime, photon-type lasing may occur, if the Bernard–Duraffourg inversion condition[6] is fulfilled, that is when the energy difference between the quasi-Fermi levels of photo-created electrons and holes exceeds the band gap energy of the active material. The photon lasing can occur under two distinctively different regimes with the gain provided by either excitons or, in the limit of strong excitation or elevated temperatures, by unbound electrons and holes (e–h plasma)[7]. Since population inversion is not needed for polariton lasing, the corresponding threshold power is expected to be orders of magnitude lower as compared to any lasing of photon type.

So far, only one or two out of these three lasing regimes have been reported for a given structure, independently of the material system examined[8–27]. Thresholds for the onset of photon lasing involving excitons have been reported as two orders of magnitude[11,12,16,18] or a factor two[19,20] greater with respect to that of polariton type. The transition from photon lasing involving excitons to photon lasing involving an e–h plasma has been evidenced only recently in the emission from ZnO-based microcavity[27]. This shows that the actual relation between all three lasing regimes has still not been established.

In the present work, we provide a comprehensive study of lasing effects in a lattice matched optical microcavity, which embeds a single CdSe/(Cd,Mg)Se quantum well (QW). Benefiting from the optimized design of the structure and from the large oscillator strength of optical transitions in II–VI semiconductors, we observe three lasing thresholds appearing consecutively with increasing excitation power at a temperature of $T = 8$ K. The first one, at an excitation power density as low as 0.75 kW cm^{-2}, is attributed to the onset of polariton lasing in the strongly coupled system. The second, occurring at an excitation power density 1.5 order of magnitude higher, represents the photon-type lasing. In this case, the strong light–matter coupling conditions are lost due to elevated optical pumping and excitons, instead of polaritons, act as the gain medium. The final threshold is observed at an excitation power yet another order of magnitude greater, and ascribed to the regime of e–h plasma type lasing. The e–h plasma lasing is maintained up to room temperature (RT) with a slight increase in the threshold power with respect to the $T = 8$ K case. These strong nonlinearities in the dependence of the emission intensity on excitation power are observed for certain, discrete points on the sample surface. We establish that the inhomogeneities, which locally enhance the light–matter interaction, are related to a disorder in the photon confining potential.

Results

Sample design. The structures are grown by molecular beam epitaxy on a ZnTe buffer layer deposited on a (100) oriented GaAs substrate. The sample design assumes that all layers are lattice matched to ZnTe with accuracy better than 1% (see Supplementary Note 1). The structure contains a 130 nm thick wedge type Cd$_{0.9}$Mg$_{0.1}$Se $\lambda/2$ microcavity ($n_{cav} = 2.7$ at $\lambda = 700$ nm) sandwiched between distributed Bragg reflectors (DBRs) made of 30 and 28.5 pairs of alternative refractive index layers, respectively for the bottom and top mirror (see Fig. 1a, b). The high refractive index layers are made of ZnTe ($n_{high} = 2.95$ at $\lambda = 700$ nm). The low refractive index layers are short period, strain compensated ZnTe|MgSe|ZnTe|MgTe superlattices[28] described by the effective refractive index $n_{low} = 2.4$ at $\lambda = 700$ nm[28,29].
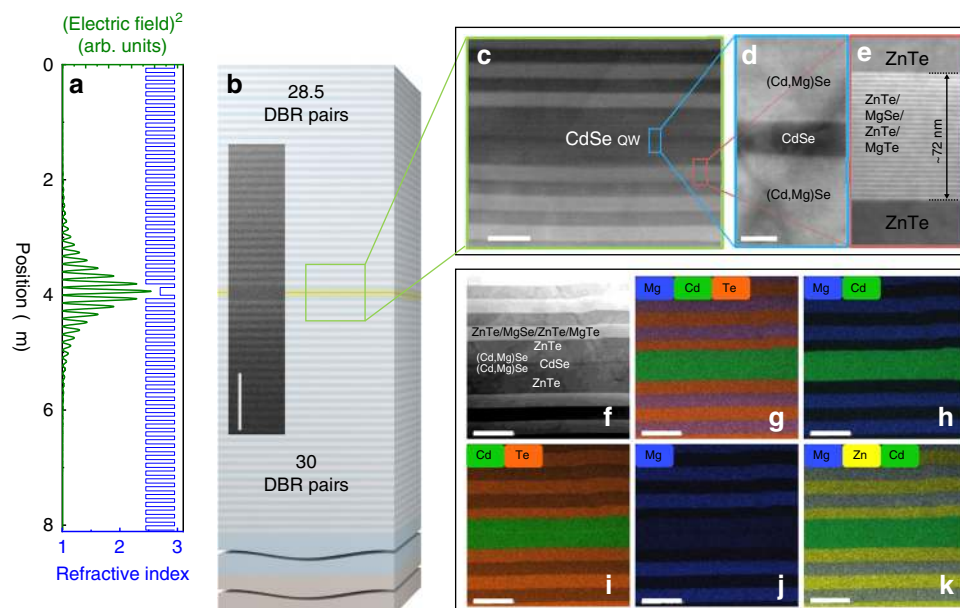
Fig. 1 Structure design. a Calculated spatial distribution of the squared electric field and a real part of the refractive index in the studied microcavity. **b** Scheme of the sample comprising a microcavity embedding a single CdSe/(Cd,Mg)Se quantum well, surrounded by a distributed Bragg reflector (DBR). A scanning electron microscopy image of the sample cross-section is shown additionally. Scale bar: 1 μm. **c** Transmission electron microscopy images of the sample showing a cross-section in the region of microcavity (scale bar: 200 nm), **d** CdSe/(Cd,Mg)Se quantum well (scale bar: 20 nm), **e** ZnTe|MgSe|ZnTe|MgTe superlattice. **f–k** Cross-sectional energy-dispersive X-ray spectroscopy images of the sample in the region of the microcavity showing a spatial distribution of Mg, Cd, Te, and Zn atoms. Scale bar: 200 nm

The nominal thickness of the DBR layers ($d_{high} = 61$ nm and $d_{low} = 73.5$ nm) is adjusted to achieve the DBRs stopband centered at $\lambda_0 = 720$ nm. A 17 nm-wide CdSe QW[30] is embedded in the center of (Cd,Mg)Se microcavity (see transmission electron microscopy (TEM) images in Fig. 1c, d), thus at the antinode of the electric field (see Fig. 1a).

The layer's thickness is monitored during the growth by in situ reflectivity. Attainment of the designed layer thickness is confirmed by the TEM images. In particular, the thickness of the superlattice is 72 nm (see Fig. 1e), close to the intended d_{low} of 73.5 nm. The TEM images reveal, however, cracks and stacking faults propagating either from the substrate layer or starting from the microcavity layer. Such defects might be responsible for additional, planar photon confinement and thus for a formation of 3D photonic traps. The chemical analysis obtained from energy-dispersive X-ray spectroscopy shows, in addition, that the layer interfaces are sharp, without a noticeable intermixing, even in the vicinity of a stacking fault, as seen in Fig. 1f–k.

Reflectivity measurements indicate that the center of a 0.25 eV wide stopband can be tuned in the spectral range between 1.7 and 1.8 eV (not shown). Due to the narrow spectral linewidth of the mode and the inhomogeneity of the structure, the reflectivity minimum related to the mode is not observed, similarly as reported previously for high-quality factor II–VI, DBR-based microcavities[13]. The linewidth of the mode determined in micro-photoluminescence (μ-PL) varies from around 5 meV to around 0.5 meV depending on the position on the sample (see Supplementary Note 2). The latter value is found only at discrete points on the sample, where the lasing emission is observed. Thus, the microcavity exhibits a quality factor ranging from a few hundreds to above $Q = 3000$, depending on the position on the sample. The estimated vacuum Rabi splitting is 5.6 ± 0.8 meV (see Supplementary Note 3), a value consistent in terms of energy per QW[31] with previous reports on II–VI microcavities embedding QWs[22,24,32–34]. At $T = 8$ K the QW emission (full width at half maximum, FWHM = 8 meV) is peaked at around 1.745 eV, while at RT it is broadened spectrally (FWHM = 85 meV) and redshifted to around 1.68 eV. The mode energy is expected to lie in the middle of the stopband, that is at around 1.72 eV (720 nm). The position on the sample is selected in such a way that the system operates at a slightly negative detuning at $T = 8$ K and close to 0 or slightly positive detuning at RT.

Electron–hole plasma lasing at 300 K. Spatial scanning of the samples μ-PL at RT reveals the presence of discrete points, where the emission is strongly enhanced and the spectrum takes the form of narrow (FWHM below 0.5 meV) lines. Figure 2 shows the evolution of the emission spectrum at such a point when the excitation power is varied from 150 to 900 kW cm^{-2}. Despite a relatively moderate increase of the excitation power (less than an order of magnitude), a highly nonlinear increase of the intensity (around four orders of magnitude) is evidenced with a threshold of about 450 kW cm^{-2} (see Fig. 3a). Approaching this threshold is accompanied by an abrupt narrowing (by almost an order of magnitude) and a significant blueshift of the emission (see Fig. 3b, c). Crossing the threshold induces a strong angular narrowing of the emission distribution (see Supplementary Note 4). Above the threshold, a slight broadening and redshift occur (see Fig. 3b, c).

Lasing at RT occurs due to a stimulated emission from a plasma of unbound, highly excited electrons and holes, as supported by following arguments: (i) thermal energy at RT (~26 meV) exceeds the exciton binding energy in a 17 nm wide CdSe QW (18 meV, see Supplementary Note 5), (ii) the injected carrier density at the lasing threshold at RT exceeds the saturation (Mott) density N_S (see Supplementary Notes 5 and 6) above
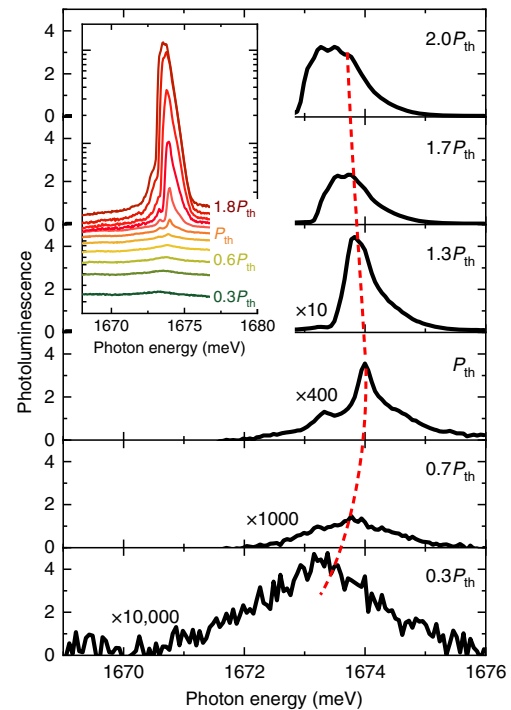

Fig. 2 Electron–hole plasma lasing at room temperature. Micro-photoluminescence spectra at $T = 300$ K for the increasing non-resonant excitation in linear and logarithmic (see inset) intensity scale. The lasing threshold power density P_{th} is 450 kW cm^{-2}. The dashed line indicates the approximated spectral position of the maximum

which excitons no longer form stable, Coulombically bound quasiparticles[35], (iii) emission dynamics measurements reveal a characteristic shift of the emission towards higher energies during the emission decay following the excitation pulse (see Supplementary Note 7), such as observed previously in the case of electron–hole plasma type lasing in ZnO nanostructures[36]. The threshold power of 450 kW cm^{-2} is smaller both in terms of photon flux per surface density (by a few times), as well as in terms of the total power of the excitation beam (by 3–4 orders of magnitude) than it was in the case of previous works involving either a single or multiple II–VI QWs[10,13] at or near RT (see Discussion).

Three types of lasing at 8 K. Remarkably, power-dependent measurements carried out at $T = 8$ K and in the location of a strongly emitting, single photonic trap reveal a nonlinear behavior exhibiting three thresholds separated by plateau regions (see the input–output dependence in Fig. 3a; the example emission spectrum at 8 K is provided in the inset to Supplementary Figure 6). The first threshold is observed at a power density of 0.75 kW cm^{-2} (12 μW of integrated power per a Gaussian spot of 2 μm diameter), the second one at 35 kW cm^{-2}, while the third one occurs at around 280 kW cm^{-2}, as indicated in Fig. 3a.

The density N_{exc} of carriers injected to the QW in a single excitation pulse corresponding to the first threshold at 8 K (0.75 kW cm^{-2}) is of the order of 10^9 cm^{-2} (see Supplementary Note 6). Such a low value allows us to identify the threshold as corresponding to the onset of polariton lasing in the strong exciton–photon coupling regime, where the bosonic nature of polaritons enables their stimulated scattering into the ground state. The threshold value found in the present case is comparable with those found in the previous studies of polariton lasing[12,16]. We note here that by term polariton lasing we mean coherent
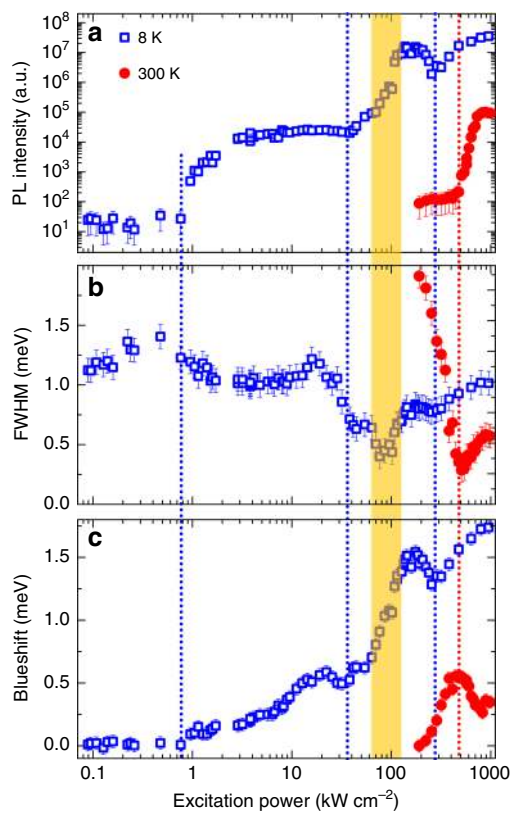
Fig. 3 Excitation power-dependent properties of emission at 8 and 300 K.
a Integrated intensity, **b** linewidth, and **c** energy blueshift of the single
photonic trap emission versus excitation power at 8 K (blue open squares)
and at 300 K (red full dots). Lasing thresholds are indicated with a dashed
vertical line. The power density for which the exciton density photo-created
in the quantum well reaches the Mott transition density is indicated with
a yellow vertical bar. Due to limited temperature stability of the setup, a
different photonic trap is studied at 8 and 300 K. Error bars determined
from a fitting procedure

light emission occurring in the strong light–matter coupling
regime involving polaritons macroscopically occupying the
ground state. We do not distinguish if we deal with the ideal
case of thermalized polariton Bose–Einstein condensate[3,14] or the
case where the full thermalization is not present (see a relevant
discussion, e.g., in ref. [5]).

With an increase of the pump power, both the exciton oscillator
strength and exciton–photon coherence gradually decrease due to
increased screening effects and a dephasing induced by the
enhanced exciton–exciton scattering. As a result, a transition from
the strong to weak exciton–photon coupling regime occurs at a
sufficiently high exciton density. We identify a second threshold
at 35 kW cm^{-2} ($N_{exc} \sim 10^{11}$ cm^{-2}, see Supplementary Note 6)
as arising from the onset of the stimulated emission of photons.
This is in line with previous studies, where the threshold of lasing
in the weak-coupling regime was shown to exceed by two orders
of magnitude that of polariton lasing[12,16,18]. Since N_{exc} is still
below the saturation value of $N_S \sim 2.4 \times 10^{11}$ cm^{-2}, determined
from the Schmitt-Rink condition[35], we conclude that the gain is
provided by excitons.

When approaching the third threshold at around 280 kW cm^{-2}
(N_{exc} of around 10^{12} cm^{-2}, see Supplementary Note 6) we
observe a narrow plateau followed by a drop of the gain in the
input–output dependence. As the injected carrier density is further
increased, a rapid nonlinear increase of the emission intensity

occurs. We have checked that the decrease of the emission
intensity below the threshold power does not result from a
competition between different modes excited by the laser spot
(see Supplementary Note 8). The drop of the gain thus indicates
that effects of Coulomb screening, phase space filling, and the
exciton–exciton exchange interaction become strong enough to
induce a complete dissociation of excitons. Since at the third
threshold N_{exc} exceeds N_S, here we encounter photon lasing
involving the stimulated recombination of the e–h plasma[7]. For a
temperature of 300 K, the threshold power density (450 kW cm^{-2})
is slightly higher, while the total emission intensity is lower
(see Fig. 3a). We ascribe this difference to the increased rate
of non-radiative processes when the temperature is raised from
8 to 300 K.

A narrowing of the emission line assists a nonlinear increase
of the emission intensity for each of the three phase transitions
(see Fig. 3b). There is also a blueshift (see Fig. 3c) that is more
pronounced in the case of the two higher thresholds, but still
present in the case of the first threshold representing the onset of
polariton-type lasing. The blueshift in the weak coupling regime
is predominantly a manifestation of the impact of increased
carrier density on the dielectric function of the microcavity layer.
A small value of the blueshift in the strong coupling regime
might result from a relatively low density of polaritons and the
exciton reservoir at the excitation of 0.75 kW cm^{-2} and pinning
of the emission to discrete energy of the state confined in the
photonic trap. A similar behavior, with only incremental blueshift
and narrowing at the threshold, has been previously reported
for polariton lasing from a discrete energy level confined in a
micropillar etched out of a GaAs-based microcavity[16,26].

Figure 3a indicates that a β-factor of the S-shaped
input–output dependence, describing the fraction of spontaneous
radiation that contributes to the lasing, is different for each of the
three lasing thresholds. Despite the fact that geometric factors
of the microcavity do not change with the excitation power, the
difference arises from the qualitatively different mechanism
of each of the three thresholds. Moreover, the lasing emission
blueshifts at around 1.5 meV in the studied excitation power
range (Fig. 3c). The spectral dependence of the β-factor and
resulting spectral dependence of the gain are expected to be
particularly significant when, as in our case, the mode energy and
associated density of photonic states exhibit discrete maxima due
to the presence of the trap.

It is worth noting that the emission linewidth of 1 meV at the
first threshold at 8 K is larger than the linewidth at the two
consecutive ones (0.6 and 0.75 meV, respectively). This can be
understood when taking into account that the linewidth of the
polariton emission in the strong coupling regime is defined by
the coupling of a spectrally wide QW and a spectrally narrow
cavity mode. On the contrary, in the weak coupling regime, the
emission exhibits a purely photonic character and the linewidth
is determined essentially by the mode linewidth. The slight
broadening at the third threshold results from dephasing effects
under strong excitation conditions.

3D light confinement in photonic traps.
As stated earlier, the
intense emission and nonlinearities in the dependence on the
excitation power are observed for discrete points on the sample.
This suggests a local increase of the lateral light confinement
in the plane of the microcavity, which enhances the interaction
between excitons and confined photons and lowers the lasing
threshold. So far, lateral photonic confinement in planar micro-
cavities have been achieved by micropillar etching[16,37], optical
excitation[38,39], application of a local strain[14,17], patterning of the
sample surface[21], or as a result of disorder in the photon
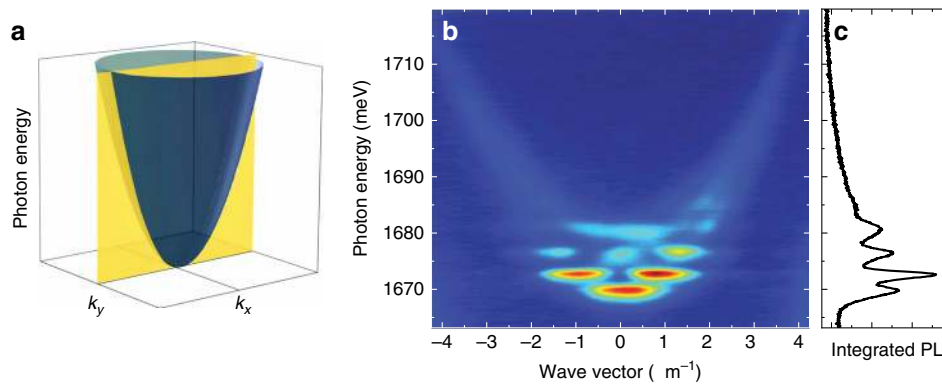
Fig. 4 Angle-resolved micro-photoluminescence—a vertical cross-section. **a** Schematic and **b** measured cross-section through in-plane photon momentum space at $k_{||} = 0$ revealing a ladder of discrete modes superimposed on a parabolic dispersion of a planar microcavity. **c** Angle-integrated emission spectrum corresponding to **b**

confining potential formed either spontaneously or introduced artificially[33,40–44].

In our case, we attribute the enhancement of the luminescence at discrete points to the presence of traps[33,42,44] resulting from inhomogeneities in the photonic potential formed spontaneously during sample growth. In order to confirm the above attribution, we perform angle-resolved μ-PL studies at the selected, strongly emitting points on the sample. We keep the temperature of experiment $T = 300$ K to ensure that polaritonic effects are negligible and properties of emission are defined predominantly by photon confinement. A typical emission spectrum of such a point under strong excitation contains a number of discrete lines. Imaging of photon in-plane momentum space (see Fig. 4) uncovers a quantized mode structure of the emission super-imposed on a typical parabolic photon momentum dispersion. This result is qualitatively similar to that reported previously for zero-dimensional photonic traps formed naturally in a CdTe-based microcavity[33,42,43], or those created intentionally in a GaAs-based microcavity[21,40]. The mode energy spacing and emission pattern of the traps are comparable to those of a micropillar with a 3–5 μm diameter, as we determined in a reference study on micropillars of various diameters etched out of a planar sample (see Supplementary Note 9). The emission at RT is linearly polarized with two orthogonal directions (see Supplementary Note 10). This indicates that the photonic trap responsible for the emission is characterized by shape anisotropy in its planar direction. Polarization directions, found to be independent of the excitation power (not shown), correspond to the principal geometry axes of the trap. We do not observe a circular polarization of the emission reported previously for e–h plasma lasing in GaAs-based microcavities[23]. This is most likely due to a large degree of photonic disorder in our samples which governs the polarization properties of the emission.

Polarization and angle-resolved tomography of the emission provide another indication that the photonic traps possess similar properties to a micropillar microcavity with an elliptical cross-section[45]. Figure 5 presents a cross-section in two orthogonal directions of the linear polarization through the in-plane photon momentum space $k_{||}$ at the energy of the first three modes. The first mode exhibits an angular emission pattern with a single maximum centered around $k_{||} = 0$ (see Fig. 5b, c). The radiation pattern of the second mode contains two maxima centered around $k_{||} = 0$ (see Fig. 5d, e), while the third mode (see Fig. 5f, g) shows three maxima. The presented radiation patterns resemble strongly those which were observed previously for micropillars with an elliptical cross-section[45,46], and natural traps formed in a planar microcavity[42].

We note that the radiation pattern of a given mode does not depend on the polarization of the emitted light, i.e., the angle distribution of the mode emission is practically the same for both orthogonal, linear polarizations of the light. This result agrees with what was previously observed in the emission from a micropillar-based photonic molecule[46].

Discussion

Strong Coulomb interactions between electrons and holes lead to a large oscillator strength of optical transitions in II–VI semiconductors, rendering them particularly suitable as an active material in photonic devices characterized by a high quantum yield and operation at elevated temperatures[8–10,13,25]. Recently, high-quality ZnSe-based microcavities enabled studies on the effect of a phonon-bath on spatial coherence of the polariton condensate for temperatures as high as 270 K[47].

The use of binary compounds for the DBRs and the QW layer should, in principle, ensure a high homogeneity of the composition, and facilitate the epitaxial growth of the structure. However, the TEM images shown in Fig. 1 indicate that despite the lattice matching between the QW, microcavity, and DBRs, a relatively high density of structure defects such as cracks or dislocations are present. This precludes achieving such high-quality factors of the microcavity and such narrow linewidths of the QW transition as in the case of previous approaches involving II–VI ternary or quaternary compounds[3,47].

The presence of photonic traps is typically an undesired feature of microcavity structures. Such traps, however, are crucial for the presented study as they allow us to decrease lasing thresholds with respect to the regular planar microcavity. This is because they yield lowered in plane photon losses than in the case of an unstructured planar microcavity[22] (see Supplementary Note 2). In the strong coupling regime, they enable, moreover, lifting of the so-called bottleneck effect, which typically significantly hinders the polariton relaxation photo-created using non-resonant excitation. The resulting acceleration of the stimulated scattering of polaritons to the lowest energy state permits condensation at lower powers[48].

In addition, bandgaps of the layers forming the DBRs are significantly (above 0.5 eV, see Supplementary Note 1) shifted toward higher energy with respect to the QW and the cavity mode energy. This makes a parasite absorption practically negligible. Moreover, the DBRs provide a reasonable refractive index contrast of 0.5 between layers forming the DBR. The $\lambda/2$ microcavity ensures the strongest possible confinement of light in the planar structure. Finally, the use of a single QW facilitates
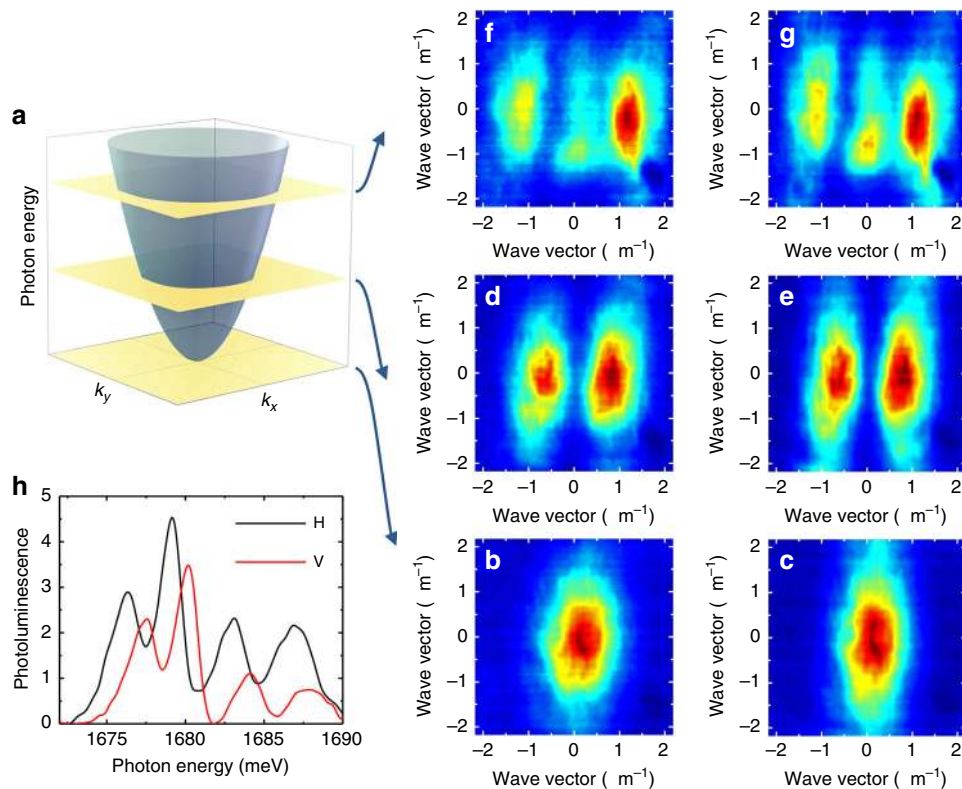
Fig. 5 Angle-resolved micro-photoluminescence—a horizontal cross-section. **a** Schematic and **b**–**g** measured cross-sections through in-plane photon momentum space at energy of the first three modes of the emission in two orthogonal linear polarizations. **h** Respective emission spectra in two orthogonal polarizations

reaching the saturation density of excitons as in our case, in the contrary to typically studied structures, the total exciton density does not undergo a distribution over several QWs. We note in addition that the studied structure can be easily grown on either ZnTe, GaSb, or InAs substrate, which is promising for the rapidly developing 6.1 Å optoelectronics[49].

The high constants of the light–matter coupling in our structures also enable us to observe RT lasing from a single QW with a very low threshold power. Previously, amplified spontaneous emission (ASE) at RT from multiple QWs made of II–VI materials such as CdTe[8] or (Cd,Zn)Se[9] have been obtained in perpendicular geometry (excitation from the top and collection of the emission from the cleaved edge of the sample). The microcavity has been formed by the edges of a stripe etched out of a planar sample without any DBRs. Later on, ASE at RT has been obtained with excitation and collection both from the top on planar vertical cavity surface-emitting laser (VCSEL) structures comprising a few (Zn,Cd)(S,Se) QWs[13] or a single ZnSe QW[10]. The power density of the lasing threshold at and near RT was of the order of 1000 kW cm^{-2}, while the excitation spot formed a stripe large for hundreds of μm by hundreds of μm. In our case, the emission is excited and collected from the top of the structure and the threshold power density of the lasing at RT is lowered to 450 kW cm^{-2}. Moreover, the diameter of the excitation spot at the sample surface is much smaller, in 1–2 μm range. This makes the threshold power of the lasing in our case smaller both in terms of photon flux per surface density (by a few times), as well as in terms of the total power of the excitation beam (by 3–4 orders of magnitude) compared to previous works involving either a single or multiple II–VI QWs[10,13] at or near RT.

Summarizing, power-dependent photoluminescence studies on an half-wavelength Se/Te-based microcavity embedding a single CdSe/(Cd,Mg)Se QW enabled us to observe three consecutive thresholds marked by a nonlinear increase of the emission intensity at $T = 8$ K. Based on the carrier density analysis we conclude that (i) an ultra-low threshold represents the onset of polariton-type lasing; (ii) a second threshold, greater by 1.5 order of magnitude, signals a transition from regime, where the lasing results from a stimulated scattering of polaritons, to the regime, where it results from a stimulated emission involving excitons; (iii) a third threshold increased by an another order of magnitude, reflects the e–h plasma photon lasing above the Mott transition for excitons. The onset of each type of lasing is accompanied by a narrowing and blueshift of the emission, which does not appear to be limited to the strong coupling regime. The e–h plasma lasing is maintained up to RT. The emission dynamics measurements at RT show a blueshift following the excitation pulse, which is in contrast to the redshift of emission typically observed in the case of polariton lasing. A photoluminescence spatial mapping indicates that nonlinear dependencies in the emission are observed only at discrete, randomly distributed points on the sample. The full tomography of photon momentum space shows that the emission from these points exhibits discrete energies and a radiation pattern such as reported previously for microcavities providing a three-dimensional light confinement. The emission remains linearly polarized at RT, when polaritonic effects are negligible. This enables tracing back the locally increased light–matter interaction to an increased light confinement in the planar direction of the microcavity, resulting from inhomogeneities formed during the sample epitaxial growth. The current study clears up a relation between lasing processes of different types in a semiconductor optical microcavity and provides an insight into the role played by native defects in this context. It also opens up the possibility to study emission coherence in terms

of the second order correlation function[20,50,51] in the full range of lasing regimes achievable in a semiconductor microcavity. We gain access to a nonequilibrium regime involving Coulomb-correlated e–h pairs above the Mott transition for excitons. This is promising for studies of many-body effects like Coulomb enhancement of gain near the Fermi energy (Fermi-edge super-radiance)[52] or studies of electron–hole pairs with resonantly enhanced oscillator strengths (Mahan excitons)[53].

Methods

μ-PL is nonresonantly excited by a Ti:sapphire laser operating in a picosecond mode, coupled to an optical parametric oscillator, which converts the infrared emission to the visible spectral range. The excitation at the energy $E_{exc} = 2.138$ eV ($\lambda_{exc} = 580$ nm) is tuned to a reflectivity minimum of the sample. At the same time, it is well below the bandgap of the materials forming the DBRs, which ensures low absorption losses of the excitation. The laser beam is focused to a 1–2 μm diameter spot at the sample surface with the use of a microscope objective (NA = 0.7) or an aspheric lens ($f = 3.1$ mm, NA = 0.68) in the case of time-integrated or time-resolved measurements, respectively. In order to avoid heating of the sample, the laser beam is chopped at 20 kHz using an acousto-optic modulator with 1% duty cycle. During low-temperature measurements, the sample is maintained in a continuous liquid helium flow cryostat at 8 K. During RT measurements, the sample is kept in open-air conditions. The combination of a half-wave plate and a linear polarizer allows for the polarization-resolved detection. A grating spectro-meter combined with a CCD camera or a streak camera serves as a detector in time-integrated or time-resolved measurements, respectively. The convolution of the Gaussian with FWHM = 12 ps and the exponential decay is fitted to the cross-section of the emission decay in order to obtain the respective decay time con-stants. The far-field distribution of the emission of the microcavity is registered by imaging the Fourier plane of the microscope objective on the entrance slit of the spectrometer. Horizontal shifting of a 300 mm lens in the direction perpendicular to the slit (50 μm step) using an automated translation stage enables the full tomography of the photon momentum parallel to the sample plane. Micropillars with a diameter from 1 to 9 μm were etched out of the planar structure using a focused ion beam in a multistage technique, in which ion beam current is varied from 9 pA to 2.7 nA (30 kV acceleration voltage) for initial etching and thinning of the micropillar down to the desired diameter, respectively. A spatial distribution of the squared electric field in the structure is calculated within the transfer matrix method formalism, assuming complex, wavelength-dependent refractive indices[28,29] of the layers.

Data availability

The data that support the findings of this study are available from the corresponding author upon reasonable request.

References

1. Diederichs, C. et al. Parametric oscillation in vertical triple microcavities. *Nature* **440**, 904–907 (2006).
2. Amo, A. et al. Superfluidity of polaritons in semiconductor microcavities. *Nat. Phys.* **5**, 805–810 (2009).
3. Kasprzak, J. et al. Bose–Einstein condensation of exciton polaritons. *Nature* **443**, 409–414 (2006).
4. Weisbuch, C., Nishioka, M., Ishikawa, A. & Arakawa, Y. Observation of the coupled exciton–photon mode splitting in a semiconductor quantum microcavity. *Phys. Rev. Lett.* **69**, 3314–3317 (1992).
5. Byrnes, T., Kim, N. Y. & Yamamoto, Y. Exciton–polariton condensates. *Nat. Phys.* **10**, 803–813 (2014).
6. Bernard, M. G. A. & Duraffourg, G. Laser conditions in semiconductors. *Phys. Status Solidi B* **1**, 699–703 (1961).
7. Klingshirn, C. & Haug, H. Optical properties of highly excited direct gap semiconductors. *Phys. Rep.* **70**, 315–398 (1981).
8. Glass, A. M. et al. Room-temperature optically pumped $Cd_{0.25}Zn_{0.75}Te/ZnTe$ quantum well lasers grown on GaAs substrates. *Appl. Phys. Lett.* **53**, 834–836 (1988).
9. Jeon, H. et al. Room-temperature blue lasing action in (Zn,Cd)Se/ZnSe optically pumped multiple quantum well structures on lattice-matched (Ga,In)As substrates. *Appl. Phys. Lett.* **57**, 2413–2415 (1990).
10. Ding, J. et al. Laser action in the blue-green from optically pumped (Zn,Cd)Se/ZnSe single quantum well structures. *Appl. Phys. Lett.* **57**, 2756–2758 (1990).
11. Dang, L. S., Heger, D., André, R., Bœuf, F. & Romestain, R. Stimulation of polariton photoluminescence in semiconductor microcavity. *Phys. Rev. Lett.* **81**, 3920 (1998).
12. Deng, H., Weihs, G., Snoke, D., Bloch, J. & Yamamoto, Y. Polariton lasing vs. photon lasing in a semiconductor microcavity. *Proc. Natl. Acad. Sci. U.S.A.* **100**, 15318–15323 (2003).
13. Kruse, C. et al. Green monolithic II–VI vertical-cavity surface-emitting laser operating at room temperature. *Phys. Status Solidi B* **241**, 731–738 (2004).
14. Balili, R., Hartwell, V., Snoke, D., Pfeiffer, L. & West, K. Bose–Einstein condensation of microcavity polaritons in a trap. *Science* **316**, 1007 (2007).
15. Christopoulos, S. et al. Room-temperature polariton lasing in semiconductor microcavities. *Phys. Rev. Lett.* **98**, 126405 (2007).
16. Bajoni, D. et al. Polariton laser using single micropillar GaAs–GaAlAs semiconductor cavities. *Phys. Rev. Lett.* **100**, 047401 (2008).
17. Nelsen, B., Balili, R., Snoke, D. W., Pfeiffer, L. & West, K. Lasing and polariton condensation: two distinct transitions in GaAs microcavities with stress traps. *J. Appl. Phys.* **105**, 122414 (2009).
18. Kammann, E., Ohadi, H., Maragkou, M., Kavokin, A. V. & Lagoudakis, P. G. Crossover from photon to exciton–polariton lasing. *New J. Phys.* **14**, 105003 (2012).
19. Tsotsis, P. et al. Lasing threshold doubling at the crossover from strong to weak coupling regime in GaAs microcavity. *New J. Phys.* **14**, 023060 (2012).
20. Tempel, J.-S. et al. Characterization of two-threshold behavior of the emission from a GaAs microcavity. *Phys. Rev. B* **85**, 075318 (2012).
21. Zhang, B. et al. Zero-dimensional polariton laser in a subwavelength grating-based vertical microcavity. *Light Sci. Appl.* **3**, e135 (2014).
22. Klein, T. et al. Polariton lasing in high-quality selenide-based micropillars in the strong coupling regime. *Appl. Phys. Lett.* **107**, 071101 (2015).
23. Hsu, F.-k, Xie, W., Lee, Y.-S., Lin, S.-D. & Lai, C.-W. Ultrafast spin-polarized lasing in a highly photoexcited semiconductor microcavity at room temperature. *Phys. Rev. B* **91**, 195312 (2015).
24. Rousset, J.-G. et al. Strong coupling and polariton lasing in te based microcavities embedding (Cd,Zn)Te quantum wells. *Appl. Phys. Lett.* **107**, 201109 (2015).
25. Lai, Y.-Y. et al. Crossover from polariton lasing to exciton lasing in a strongly coupled ZnO microcavity. *Sci. Rep.* **6**, 20581 (2016).
26. Sala, V. G. et al. Stochastic precession of the polarization in a polariton laser. *Phys. Rev. B* **93**, 115313 (2016).
27. Niyuki, R. et al. Double threshold behavior in a resonance-controlled ZnO random laser. *APL Photonics* **2**, 036101 (2017).
28. Pacuski, W., Kruse, C., Figge, S. & Hommel, D. High-reflectivity broadband distributed Bragg reflector lattice matched to ZnTe. *Appl. Phys. Lett.* **94**, 191108 (2009).
29. Rousset, J.-G. et al. MBE grown microcavities based on selenium and tellurium compounds. *J. Cryst. Growth* **401**, 499–503 (2014).
30. Rudniewski, R. et al. Type I CdSe and CdMgSe quantum wells. *Acta Phys. Pol. A* **126**, 1167 (2014).
31. Savona, V., Andreani, L., Schwendimann, P. & Quattropani, A. Quantum well excitons in semiconductor microcavities: unified treatment of weak and strong coupling regimes. *Solid State Commun.* **93**, 733–739 (1995).
32. Bleuse, J. et al. Laser emission on a cavity-polariton line in a II–VI microcavity. *J. Cryst. Growth* **184**, 750–753 (1998).
33. Sanvitto, D. et al. Exciton–polariton condensation in a natural two-dimensional trap. *Phys. Rev. B* **80**, 045301 (2009).
34. Sebald, K. et al. Strong coupling in monolithic microcavities with ZnSe quantum wells. *Appl. Phys. Lett.* **100**, 161104 (2012).
35. Schmitt-Rink, S., Chemla, D. S. & Miller, D. A. B. Theory of transient excitonic optical nonlinearities in semiconductor quantum-well structures. *Phys. Rev. B* **32**, 6601–6609 (1985).
36. Takeda, J., Kurita, S., Chen, Y. & Yao, T. Ultrafast carrier dynamics in ZnO epitaxial thin films studied by optical Kerr gate luminescence spectroscopy. *Int. J. Mod. Phys. B* **15**, 3669–3672 (2001).
37. Bloch, J. et al. Strong and weak coupling regime in pillar semiconductor microcavities. *Physica E* **2**, 915–919 (1998).
38. Roumpos, G., Nitsche, W. H., Höfling, S., Forchel, A. & Yamamoto, Y. Gain-induced trapping of microcavity exciton polariton condensates. *Phys. Rev. Lett.* **104**, 126403 (2010).
39. Askitopoulos, A. et al. Polariton condensation in an optically induced two-dimensional potential. *Phys. Rev. B* **88**, 041308(R) (2013).
40. Daïf, O. E. et al. Polariton quantum boxes in semiconductor microcavities. *Appl. Phys. Lett.* **88**, 061105 (2006).
41. Nardin, G., Léger, Y., Pietka, B., Morier-Genoud, F. & Deveaud-Plédran, B. Phase-resolved imaging of confined exciton-polariton wave functions in elliptical traps. *Phys. Rev. B* **82**, 045304 (2010).
42. Zajac, J. M., Langbein, W., Hugues, M. & Hopkinson, M. Polariton states bound to defects in GaAs/AlAs planar microcavities. *Phys. Rev. B* **85**, 165309 (2012).

43. Ding, F., Stöferle, T., Mai, L., Knoll, A. & Mahrt, R. F. Vertical microcavities with high Q and strong lateral mode confinement. *Phys. Rev. B* **87**, 161116 (2013).

44. Thunert, M. et al. Cavity polariton condensate in a disordered environment. *Phys. Rev. B* **93**, 064203 (2016).

45. Sebald, K., Seyfried, M., Klembt, S. & Kruse, C. Optical properties of photonic molecules and elliptical pillars made of ZnSe-based microcavities. *Opt. Express* **19**, 19422–19429 (2011).

46. Dousse, A. et al. Ultrabright source of entangled photon pairs. *Nature* **466**, 217 (2010).

47. Klembt, S., Stepanov, P., Klein, T., Minguzzi, A. & Richard, M. Thermal decoherence of a nonequilibrium polariton fluid. *Phys. Rev. Lett.* **120**, 035301 (2018).

48. Schneider, C. et al. Exciton–polariton trapping and potential landscape engineering. *Rep. Prog. Phys.* **80**, 016503 (2017).

49. Fan, J. et al. Growth and material properties of ZnTe on GaAs, InP, InAs and GaSb (0 0 1) substrates for electronic and optoelectronic device applications. *J. Cryst. Growth* **323**, 127–131 (2011).

50. Kim, S. et al. Coherent polariton laser. *Phys. Rev. X* **6**, 011026 (2016).

51. Klaas, M. et al. Photon-number-resolved measurement of an exciton–polariton condensate. *Phys. Rev. Lett.* **121**, 047401 (2018).

52. Kim, J.-H. et al. Fermi-edge superfluorescence from a quantum-degenerate electron–hole gas. *Sci. Rep.* **3**, 061105 (2013).

53. Mahan, G. D. Excitons in degenerate semiconductors. *Phys. Rev.* **153**, 882–889 (1967).

Acknowledgements

Author contributions

K. S. and J.S. were involved in all steps of this work apart from the sample growth and initial PL measurements. R.R. and W.P. epitaxially grew the samples. J.-G.R. with W.P. initiated the PL measurements on the studied samples. M.Ś. and T.K. participated in optical measurements. K. Sobczak and J.B. performed transmission electron microscopy measurements. M.N. participated in design of the studies, interpretation of the results, and the manuscript preparation. All authors reviewed the manuscript.

Additional information

Competing interests: The authors declare no competing interests.

Reprints and permission information is available online at http://npg.nature.com/reprintsandpermissions/

Publisher's note: Springer Nature remains neutral with regard to jurisdictional claims in published maps and institutional affiliations.